

Effects of particles with large gyroradii on resistive magnetohydrodynamic stability

V. A. Svidzinski and S. C. Prager

University of Wisconsin-Madison, Madison, Wisconsin 53706

(Received 19 September 2003; accepted 25 November 2003)

Fast ions in tokamaks are known to have a significant influence on global plasma instabilities. In normal mode analyses for tokamaks, the perturbed electric and magnetic fields have been evaluated at the position of the particle's guiding center. The effect of spatial variation of the perturbed fields *within* the gyroradius for resistive internal magnetohydrodynamic (MHD) modes is considered in the present paper. The resulting tearing mode stability for the reversed field pinch (RFP) is investigated. Such effects are important for neutral beam injected particles in current RFP experiments and for fusion-generated alpha particles. The fast particle dielectric response is evaluated from the linearized Vlasov equation, and inserted into a cylindrical MHD model for the bulk plasma. The response is found for the simplified particles distribution function assuming that equilibrium magnetic field is uniform within the gyro-orbit. The effect of large gyroradii is strong, and can be either stabilizing or destabilizing (depending on the radial distribution of the fast particle density). The effect is maximal when the fast particles reside near the tearing-resonant surface. © 2004 American Institute of Physics. [DOI: 10.1063/1.1643058]

I. INTRODUCTION

Fast ions in tokamaks have been found to have a significant influence on the dynamics of global plasma stability. The effect can be stabilizing or destabilizing. The destabilizing influence has been observed in fishbone oscillations of neutral beam injected (NBI) plasmas; the stabilizing influence has been observed in the Joint European Torus tokamak in which fast ions are produced by radio frequency heating (see review by Porcelli¹).

In normal mode analyses of tokamak plasmas with low poloidal and toroidal mode numbers the fast ion response has been described by the linearized Vlasov equation in which an expansion over the parameter $\epsilon = \rho_L/a$ is made, where ρ_L is fast ion Larmor radius and a is the minor radius.²⁻⁴ The finite Larmor radius (FLR) terms starting from ϵ^2 are neglected in the analysis; thus the effects due to spatial variation of perturbed fields within the gyroradius are not considered. Exactly these effects we call FLR effects in our study. The neglect of FLR effects has been motivated by two reasons. First, the gyroradii are typically larger than the resistive (reconnection) layer width. Hence, it is argued that the influence of the large gyroradius particles is suppressed through orbit-averaging over an oscillatory radial wave function. Second, the gyroradii can be much smaller than the perpendicular wavelengths, so that the wave fields can be considered to be constant within a gyrodiameter. However, the present work suggests that these arguments may not apply, and finite gyroradius effects may be important, for some tokamak cases of interest, such as tokamaks with particles in the MeV range.

The FLR effects may be particularly important for the reversed field pinch (RFP). In reversed field pinches the magnetic field is an order of magnitude smaller than in tokamaks. For example, in the Madison Symmetric Torus (MST)

experiment,⁵ the Larmor diameter of fast ions arising from NBI (at 20 keV) is about one third of the minor radius. The perpendicular wave length of global plasma modes is comparable to the Larmor radius of fast particles. Thus the finite Larmor radius effects mentioned above can be important. The nonlocality of the FLR fast particle response introduces complication in the modeling. In RFPs these FLR effects (which survive in the limit of homogeneous equilibrium magnetic field) should be addressed along with the effects of the inhomogeneity (particle drifts, toroidal trapping). The latter are extensively studied in tokamaks.

In our linear mode analysis we concentrate on FLR effects only and evaluate the stability of resistive internal current-driven magnetohydrodynamic (MHD) modes. We use the Vlasov equation to calculate the fast particles current driven by the perturbed electric and magnetic fields assuming that the equilibrium magnetic field is uniform within the gyro-orbit. Our analysis is a special case of the general approach suggested by Brambilla⁶ for finding the low frequency plasma response by integrating the linearized Vlasov equation along the unperturbed orbits.

We consider a cylindrical plasma and a simple fast ion distribution function

$$F(\mathbf{v}) = \frac{1}{2\pi v_0} \delta(v_\perp - v_0) \cdot \frac{1}{\sqrt{\pi} v_T} \exp(-v_\parallel^2/v_T^2)$$

with the assumption $v_T \ll v_0$. This approximates the distribution of perpendicularly injected fast ions, makes it possible to find the conductivity kernel analytically, and retains the FLR feature. The fast ion current, driven by the perturbed electric and magnetic field, is inserted into the MHD equations to find the changes to the tearing instability with poloidal wave number $m=1$ in the RFP.

Our results show that for typical neutral beam injected fast particle densities (a few percent of the bulk density) the changes to the growth rates are substantial. The effect can be stabilizing or destabilizing depending on the radial distribution of fast particles. Results depend strongly on the particle's Larmor radius. The FLR effects alone can significantly change the mode dynamics in RFP. The result is influenced by the presence of fast particles inside the transition layer (the effect which considered to be negligible in tokamak modeling). Finite spread in parallel velocity of fast particles reduces the effect in our model. This reduction is probably less significant when particle's trapping is included.

Section II contains an analysis of internal modes without fast particles. In Sec. III we derive the conductivity kernel for calculation of fast particles current. In Sec. IV we combine fast particles component with plasma bulk. This section also contains a description of the approach used for solving the combined system. In Sec. V we present the results of our study. We summarize in Sec. VI.

II. CURRENT DRIVEN MODES WITHOUT FAST PARTICLES

First we develop the numerical method for finding internal cylindrical eigenmodes in an RFP equilibrium. We consider the resistive MHD model (see, e.g., Ref. 7) in the limit of zero plasma pressure for the description of the plasma bulk. We normalize variables such that

$$r = a\tilde{r}, \quad B = B_0\tilde{B}, \quad E = \frac{v_A}{c}B_0\tilde{E}, \quad J = \frac{c}{4\pi} \frac{B_0}{a} \tilde{J},$$

$$v_A = \frac{B_0}{\sqrt{4\pi\rho_0}},$$

$$\omega = \frac{\tilde{\omega}}{\tau_A}, \quad \tau_A = \frac{a}{v_A}, \quad \rho = \rho_0\tilde{\rho}, \quad \eta = \eta_0\tilde{\eta},$$

$$S = \frac{\tau_R}{\tau_A}, \quad \tau_R = \frac{4\pi a^2}{c^2\eta_0},$$

where a is the radius of the cylinder, B_0 , ρ_0 , η_0 are equilibrium magnetic field, plasma density and plasma resistivity at $r=0$ and S is the Lundquist number. In all of the following equations in this section the variables are normalized.

We consider a force free equilibrium in which

$$\nabla \times \mathbf{B} = \mu(r)\mathbf{B}. \tag{1}$$

Azimuthally and axially symmetric solution of Eq. (1) gives equilibrium field components $\bar{B}_r=0$, $\bar{B}_\theta(r)$, $\bar{B}_z(r)$. We linearize resistive MHD equations about this equilibrium. Assuming time dependence proportional to $e^{-i\omega t}$ equations for the perturbed quantities are

$$\mathbf{E} + \mathbf{v} \times \bar{\mathbf{B}} = \frac{\tilde{\eta}}{S} \mathbf{J}, \tag{2}$$

$$-i\omega\tilde{\rho}\mathbf{v} = \tilde{\mathbf{J}} \times \mathbf{B} + \mathbf{J} \times \bar{\mathbf{B}}, \tag{3}$$

$$\nabla \times \mathbf{E} = i\omega\mathbf{B}, \tag{4}$$

$$\nabla \times \mathbf{B} = \mathbf{J}. \tag{5}$$

Equations (2)–(5) are Fourier analyzed so that spatial dependence proportional to $e^{im\theta+ikz}$ is considered. The boundary value problem for the plasma eigenmodes is defined by Eqs. (2)–(5), and by the boundary conditions on axis and on the surface of the perfectly conducting shell. On axis field components are regular and at $r=1$ $E_\theta(1)=0$, $E_z(1)=0$. We convert field components into a local coordinate frame connected with the equilibrium magnetic field. The triad of unit vectors of this frame is \mathbf{e}_r , $\mathbf{e}_\eta = \mathbf{b} \times \mathbf{e}_r$, $\mathbf{e}_\parallel = \mathbf{b}$, where $\mathbf{b} = \bar{\mathbf{B}}/\bar{B}$. From Eqs. (2)–(5) we obtain a set of rather bulky equations for Fourier amplitudes B_r , B_η , B_\parallel corresponding to wave numbers m and k . These equations contain an algebraic equation for B_r , and two second order differential equations for B_η and B_\parallel with coefficients containing derivatives of equilibrium field components.

The location of the resonance surface r_s is defined by $k_\parallel(r_s)=0$ where

$$k_\parallel = \mathbf{k} \cdot \mathbf{b} = \frac{m}{r} \frac{\bar{B}_\theta}{\bar{B}} + k \frac{\bar{B}_z}{\bar{B}}.$$

To find the eigenmode we match solutions found in the regions $0 \leq r \leq r_s$ and $r_s \leq r \leq 1$ at the resonance point as follows. Applying two sets of boundary conditions at $r=r_s$ $B_\eta(r_s)=1$, $B_\parallel(r_s)=0$ and $B_\eta(r_s)=0$, $B_\parallel(r_s)=1$ for fixed ω we find the corresponding solutions of differential equations in these two regions which are subject to the boundary conditions at $r=0$ and $r=1$. These solutions are found numerically by a finite difference method. Continuity of current components J_η and J_\parallel at $r=r_s$ (which is equivalent to continuity of B'_η and B'_\parallel) applied to an arbitrary linear combination of the two solutions leads to a set of two uniform algebraic equations for the unknown coefficients of the linear combination. Then we scan frequency ω to find the eigenvalue for which the equations have a solution. For the found eigenvalue relation between the coefficients provides the necessary relation between B_η and B_\parallel at $r=r_s$.

In this approach equations based on the resistive MHD model are solved on the entire interval $0 \leq r \leq 1$. Such an approach is more numerically intensive than the one in which resistive MHD equations are solved in the vicinity of the resonance surface and the ideal MHD equations are used in the rest of the plasma. Introduction of the nonlocal fast particle response is more simple, however, in the model in which one type of equations is used everywhere in the plasma.

One should also note that matching solutions at the resonant surface is more appropriate for numerical analysis than the adjustment of boundary conditions at $r=1$. In the latter case an arbitrary boundary condition at $r=1$ excites (in the resistive MHD model) a very rapidly growing solution in the region outside the resonance layer resulting in a stiff matrix in the eigenvalue analysis.

The equilibrium current profile is parametrized such that $\mu = 2\Theta_0[1-(r/a)^{\alpha_0}]$. We also assume that $\tilde{\rho}(r)=1$ and $\tilde{\eta}(r)=1$. A stability diagram for the $m=1$ modes in the $\alpha_0-\Theta_0$ plane is presented in Ref. 8. We reproduced this diagram here in Fig. 1. We analyze the effects of fast par-

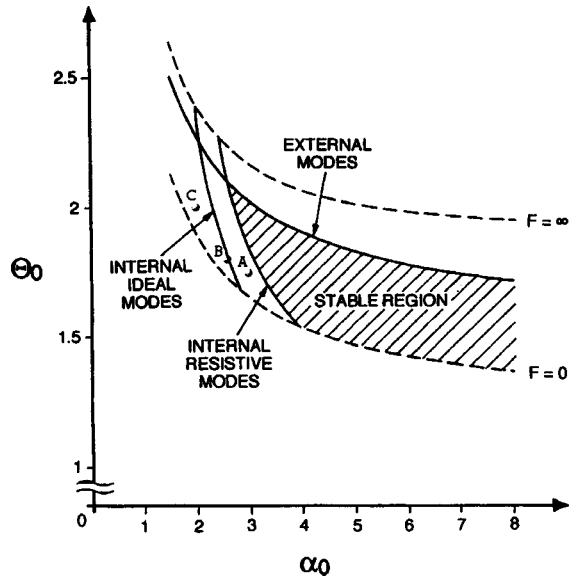


FIG. 1. Stability diagram for $m=1$ modes. [V. Antoni, D. Merlin, S. Ortolani, and R. Paccagnella, Nucl. Fusion **26**, 1711 (1986).]

ticles on the modes in the unstable region of the diagram. In the following sections we will focus on points A ($\alpha_0=3$, $\Theta_0=1.75$), B ($\alpha_0=2.6$, $\Theta_0=1.8$), and C ($\alpha_0=2$, $\Theta_0=2$) on the diagram in Fig. 1.

Figure 2 shows the radial profiles of field components of tearing mode for equilibrium A for two Lundquist numbers. The field components are in arbitrary units but their relative magnitudes are preserved. Magnetic and electric field components calculated with $S=10^4$ are presented on Figs. 2(a) and 2(b). The components calculated with $S=10^5$ are presented in Figs. 2(c) and 2(d). The wave numbers for these figures are $m=1$ and $ka=-2$. For $S=10^4$ the growth rate of the tearing mode is $\gamma\tau_A=1.10\times 10^{-3}$, for $S=10^5$ $\gamma\tau_A=6.40\times 10^{-4}$. Electric field components of the mode are localized near the resonance surface (the same is true for E_{\parallel} which is much smaller than E_r , E_{η} and is not presented in these figures) while magnetic field components are spread over the entire plasma. The electric field is more localized for larger S . The growth rate scales as $\gamma\propto S^{-2/5}$ when $S\rightarrow\infty$. The mode structure for equilibriums B and C is similar to the one presented in Fig. 2.

III. FAST PARTICLE RESPONSE

In this section we evaluate the fast particle response to a perturbation of the electromagnetic field. For the time of the mode growth fast ions are collisionless. We concentrate on finite Larmor radius effects only and find the linear nonlocal dielectric response of a population of fast ions in a uniform magnetic field. In the following sections we will use this response to calculate the changes to the internal modes in RFP. With this simplification a reasonable accuracy is preserved when particles are distributed not far from the magnetic axis.

Let $\bar{\mathbf{B}}\parallel\mathbf{z}$, then in general in the uniform magnetic field the relation between the perturbed current of fast ions and

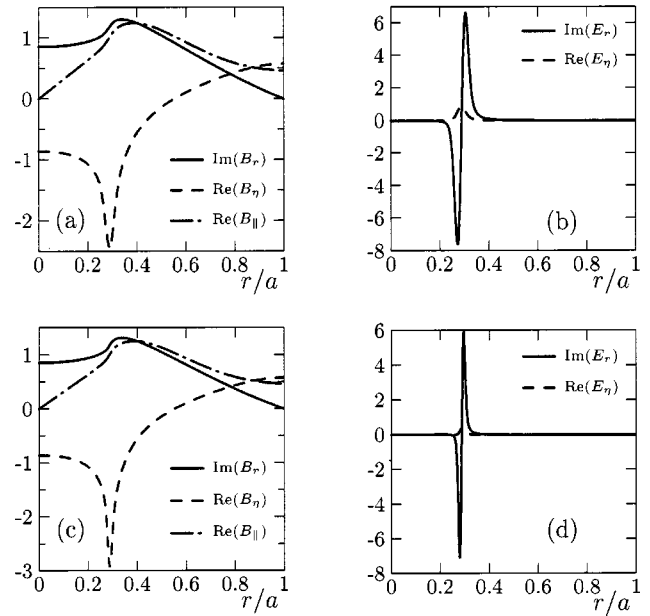


FIG. 2. Field components of tearing mode (in arbitrary units). (a),(b) $S=10^4$; (c),(d) $S=10^5$. In all cases $\alpha_0=3$, $\Theta_0=1.75$, $m=1$, $ka=-2$.

perturbed electric and magnetic fields with wave number k_z is

$$J_i(x=0,y=0,k_z) = \int_{-\infty}^{\infty} \int_{-\infty}^{\infty} dx dy \sigma_{ij}^E(x,y) E_j(x,y) + \int_{-\infty}^{\infty} \int_{-\infty}^{\infty} dx dy \sigma_{ij}^B(x,y) B_j(x,y). \tag{6}$$

In this equation $i,j=x,y,z$. The conductivity kernels σ_{ij}^E and σ_{ij}^B which are to be found are functions of coordinates x, y which are defined in a vicinity of point labeled $x=0, y=0$. Magnetic field in Eq. (6) can be expressed in terms of electric field using Maxwell equation $\nabla\times\mathbf{E}=(i\omega/c)\mathbf{B}$. We keep, however, the separate contribution from electric and magnetic fields as in Eq. (6). In this form the kernel components are more simple and more suitable for numerical analysis.

First we consider kernels σ_{ij}^E and σ_{ij}^B in Fourier representation such that

$$J_i(k_x,k_y) = \sigma_{ij}^E(k_x,k_y) E_j(k_x,k_y) + \sigma_{ij}^B(k_x,k_y) B_j(k_x,k_y),$$

where k_x, k_y are the wave numbers corresponding to coordinates x, y . For a general distribution function of fast ions $F(v_{\perp}, v_{\parallel})$ and for $\mathbf{k}=k_{\perp}\mathbf{e}_x+k_{\parallel}\mathbf{e}_z$ the conductivity tensor is found by the integration of the linearized Vlasov equation along the unperturbed particles orbits (see, e.g., Ref. 9),

$$\sigma_{ij}^{E,M}(\mathbf{k}, \omega) = -\frac{1}{4\pi i} \frac{\omega_{pi}^2}{\omega} \int_0^\infty v_\perp dv_\perp \int_{-\infty}^\infty dv_\parallel \left[2\pi \sum_{n=-\infty}^{+\infty} \frac{\omega}{\omega - n\omega_{ci} - k_\parallel v_\parallel} Q_{ij}^{nE,M}(v_\perp, v_\parallel, \mathbf{k}, \omega) \right], \tag{7}$$

with

$$\begin{aligned} Q_{xx}^{nE} &= -\frac{n^2}{\xi_\perp^2} J_n^2(\xi_\perp) v_\perp \frac{\partial F}{\partial v_\perp}, \\ Q_{xy}^{nE} &= -Q_{yx}^{nE} = -i \frac{n}{\xi_\perp} J_n(\xi_\perp) J'_n(\xi_\perp) v_\perp \frac{\partial F}{\partial v_\perp}, \\ Q_{xz}^{nE} &= -\frac{n}{\xi_\perp} J_n^2(\xi_\perp) v_\perp \frac{\partial F}{\partial v_\parallel}, \\ Q_{yy}^{nE} &= -J_n'^2(\xi_\perp) v_\perp \frac{\partial F}{\partial v_\perp}, \\ Q_{yz}^{nE} &= i J_n(\xi_\perp) J'_n(\xi_\perp) v_\perp \frac{\partial F}{\partial v_\parallel}, \\ Q_{zx}^{nE} &= -\frac{n}{\xi_\perp} J_n^2(\xi_\perp) v_\parallel \frac{\partial F}{\partial v_\perp}, \\ Q_{zy}^{nE} &= -i J_n(\xi_\perp) J'_n(\xi_\perp) v_\parallel \frac{\partial F}{\partial v_\perp}, \\ Q_{zz}^{nE} &= -J_n^2(\xi_\perp) v_\parallel \frac{\partial F}{\partial v_\parallel}, \\ Q_{xx}^{nM} &= Q_{yy}^{nM} = i \frac{n}{\xi_\perp} J_n(\xi_\perp) J'_n(\xi_\perp) \frac{v_\perp}{c} \Theta_v F, \\ Q_{xy}^{nM} &= -\frac{n^2}{\xi_\perp^2} J_n^2(\xi_\perp) \frac{v_\perp}{c} \Theta_v F, \\ Q_{yx}^{nM} &= J_n'^2(\xi_\perp) \frac{v_\perp}{c} \Theta_v F, \quad Q_{xz}^{nM} = 0, \quad Q_{yz}^{nM} = 0, \\ Q_{zx}^{nM} &= i J_n(\xi_\perp) J'_n(\xi_\perp) \frac{v_\parallel}{c} \Theta_v F, \\ Q_{zy}^{nM} &= -\frac{n}{\xi_\perp} J_n^2(\xi_\perp) \frac{v_\parallel}{c} \Theta_v F, \quad Q_{zz}^{nM} = 0, \end{aligned}$$

where

$$\xi_\perp = \frac{k_\perp v_\perp}{\omega_{ci}}, \quad \Theta_v F = v_\perp \frac{\partial F}{\partial v_\parallel} - v_\parallel \frac{\partial F}{\partial v_\perp}$$

and J_n are the Bessel functions. In Eq. (7) ω_{pi} and ω_{ci} are the plasma and cyclotron frequency of fast ions.

We consider a simple distribution function of fast particles

$$\begin{aligned} F(\mathbf{v}) &= \frac{1}{2\pi v_0} \delta(v_\perp - v_0) \cdot \frac{1}{\sqrt{\pi} v_T} e^{-v_\parallel^2/v_T^2}, \\ 2\pi \int_0^\infty dv_\perp v_\perp \int_{-\infty}^\infty dv_\parallel F(\mathbf{v}) &= 1, \end{aligned} \tag{8}$$

where v_\perp, v_\parallel are velocity components in cylindrical coordinates. Such a choice of the distribution function permits an analytic calculation of the conductivity kernels in Eq. (6) and it is appropriate for focusing on the FLR effects which are related to the perpendicular part of the distribution function. We retain some Gaussian spread in parallel velocity which is relevant to realistic distribution functions and can influence significantly the results of our study. We consider, however, the cases in which $v_T \ll v_0$.

In our case the growth rate of the mode is much smaller than the cyclotron frequency of fast ions. There is a small parameter $\varepsilon = |\omega|/\omega_{ci}$. Careful analysis shows that for the given perturbed field amplitudes presented in Fig. 2 the dominant contribution to the perturbed fast particles current is due to components $\sigma_{yy}^E, \sigma_{xy}^E, \sigma_{yx}^E, \sigma_{yx}^M, \sigma_{zx}^M$. The response due to the other components is at least by the factor ε smaller and they are not considered in our analysis.

Substituting the distribution function of Eq. (8) into Eq. (7), and using $\varepsilon \ll 1$ and $k_\parallel v_T \ll \omega_{ci}$ one obtains

$$\begin{aligned} \sigma_{yy}^E(\mathbf{k}, \omega) &= \frac{1}{2\pi i} \frac{\omega_{pi}^2}{\omega} \xi_{\perp 0} J_0(\xi_{\perp 0}) J_1(\xi_{\perp 0}) \\ &\cdot \frac{\omega}{|k_\parallel| v_T} Z\left(\frac{\omega}{|k_\parallel| v_T}\right), \end{aligned} \tag{9}$$

$$\begin{aligned} \sigma_{xy}^E(\mathbf{k}, \omega) &= -\sigma_{yx}^E(\mathbf{k}, \omega) \\ &= \frac{1}{4\pi} \frac{\omega_{pi}^2}{\omega_{ci} \xi_{\perp 0}} [J_0(\xi_{\perp 0}) J_1(\xi_{\perp 0}) \xi_{\perp 0}]', \end{aligned} \tag{10}$$

$$\begin{aligned} \sigma_{yx}^M(\mathbf{k}, \omega) &= \frac{1}{4\pi i} \frac{\omega_{pi}^2}{\omega} \frac{k_\parallel v_0^2}{\omega c} J_1^2(\xi_{\perp 0}) \\ &\cdot \left(\frac{\omega}{|k_\parallel| v_T}\right)^2 Z'\left(\frac{\omega}{|k_\parallel| v_T}\right), \end{aligned} \tag{11}$$

$$\begin{aligned} \sigma_{zx}^M(\mathbf{k}, \omega) &= -\frac{1}{4\pi} \frac{\omega_{pi}^2}{\omega} \frac{v_0}{c} J_0(\xi_{\perp 0}) J_1(\xi_{\perp 0}) \\ &\cdot \left(\frac{\omega}{|k_\parallel| v_T}\right)^2 Z'\left(\frac{\omega}{|k_\parallel| v_T}\right), \end{aligned} \tag{12}$$

where $\xi_{\perp 0} = k_\perp v_0/\omega_{ci}$ and Z is the plasma dispersion function. In our case of energetic ions $\xi_{\perp 0}$ is not a small parameter. In Eq. (9) we neglected the terms which survive when $\xi_{\perp 0} \rightarrow 0$ (they correspond to polarization drift of particle in the perturbed field) because they are of the order of $\varepsilon^2 \omega_{pi}^2/\omega$. The component $\sigma_{yy}^E(\mathbf{k}, \omega)$ in the context of waves in plasmas is responsible for the transit time magnetic pumping effect which is the FLR effect remaining finite in the limit $\varepsilon \rightarrow 0$.

The conductivity tensor components describe particle motion in a field which can vary significantly within a gyroradius, the case of interest here. In the limit of small gyroradii

dius ($\xi_{\perp 0} \ll 1$) and zero parallel velocity ($v_T \rightarrow 0$), the current obtained from the conductivity tensor contains both single particle guiding center drifts and effects that arise only with a distribution of particles (such as magnetization currents). In the small gyroradius limit, the σ_{xy}^E component reduces to $\mathbf{E} \times \bar{\mathbf{B}}$ drift in the wave electric field and the σ_{zx}^M component reduces to the $-\boldsymbol{\mu} \nabla \mathbf{B}$ force (where $\boldsymbol{\mu}$ is the magnetic moment). The other two components in Eqs. (9)–(12) do not yield currents that can be reduced to known single particle drifts.

Transformation of the conductivity kernels from Fourier representation to x, y coordinates involves integrals of Bessel functions

$$\int_0^\infty x J_0(x) J_1(x) J_1(bx) dx = \begin{cases} \frac{1}{\pi \sqrt{2^2 - b^2}}, & 0 < b < 2, \\ 0, & b > 2, \end{cases} \quad (13)$$

$$\int_0^\infty J_1^2(x) J_1(bx) dx = \begin{cases} \frac{1}{2\pi} \sqrt{2^2 - b^2}, & 0 < b < 2, \\ 0, & b > 2. \end{cases} \quad (14)$$

These integrals can be found in Ref. 10. An elegant property of these integrals is that the result of integration is nonzero within a limited range of the parameter b . This property is directly related to the fact that the conductivity kernels are nonzero within the particle's Larmor diameter from the point where the current is calculated. In the Appendix we present the details of the derivation of the contribution to the conductivity kernel $\sigma_{ij}^E(x, y)$ due to the $\sigma_{yy}^E(\mathbf{k}, \omega)$ component of the conductivity tensor in Fourier representation. The contributions from the other components of Eqs. (10)–(12) are calculated in a similar way. The result is

$$\sigma_{yy}^E: \begin{bmatrix} J_x(0,0) \\ J_y(0,0) \end{bmatrix} = -\frac{i}{(2\pi)^2} \frac{\omega_{pi}^2}{\omega} \cdot \frac{\omega}{|k_{\parallel} v_T} Z \left(\frac{\omega}{|k_{\parallel} v_T} \right) \int_0^{2\pi} d\theta \int_0^{2v_0/\omega_{ci}} dr \cdot \frac{\omega_{ci}}{v_0} \frac{1}{\pi \sqrt{2^2 - \left(\frac{\omega_{ci} r}{v_0}\right)^2}} \times \left\{ \begin{bmatrix} \cos \theta \\ \sin \theta \end{bmatrix} E_r(r, \theta) + \begin{bmatrix} \sin \theta \\ -\cos \theta \end{bmatrix} \frac{\partial [r E_\theta(r, \theta)]}{\partial r} \right\}, \quad (15)$$

$$\sigma_{xy}^E, \sigma_{yx}^E: \begin{bmatrix} J_x(0,0) \\ J_y(0,0) \end{bmatrix} = \frac{1}{8\pi^3} \frac{\omega_{pi}^2}{v_0} \int_0^{2\pi} d\theta \int_0^{2v_0/\omega_{ci}} dr \left(\frac{\omega_{ci} r}{v_0} \right)^2 \frac{1}{\sqrt{2^2 - \left(\frac{\omega_{ci} r}{v_0}\right)^2}} \begin{bmatrix} \sin \theta & \cos \theta \\ -\cos \theta & \sin \theta \end{bmatrix} \begin{bmatrix} E_r(r, \theta) \\ E_\theta(r, \theta) \end{bmatrix}, \quad (16)$$

$$\sigma_{yx}^M: \begin{bmatrix} J_x(0,0) \\ J_y(0,0) \end{bmatrix} = \frac{i}{16\pi^3} \frac{\omega_{pi}^2}{\omega} \frac{k_{\parallel} v_0}{\omega} \frac{\omega_{ci}}{c} \cdot \left(\frac{\omega}{|k_{\parallel} v_T} \right)^2 Z' \left(\frac{\omega}{|k_{\parallel} v_T} \right) \times \int_0^{2\pi} d\theta \int_0^{2v_0/\omega_{ci}} dr \begin{bmatrix} \left(\frac{\omega_{ci} r}{v_0}\right)^2 & \\ -\sin \theta \frac{\left(\frac{\omega_{ci} r}{v_0}\right)^2}{\sqrt{2^2 - \left(\frac{\omega_{ci} r}{v_0}\right)^2}} & \cos \theta \sqrt{2^2 - \left(\frac{\omega_{ci} r}{v_0}\right)^2} \\ \left(\frac{\omega_{ci} r}{v_0}\right)^2 & \\ \cos \theta \frac{\left(\frac{\omega_{ci} r}{v_0}\right)^2}{\sqrt{2^2 - \left(\frac{\omega_{ci} r}{v_0}\right)^2}} & \sin \theta \sqrt{2^2 - \left(\frac{\omega_{ci} r}{v_0}\right)^2} \end{bmatrix} \begin{bmatrix} B_r(r, \theta) \\ B_\theta(r, \theta) \end{bmatrix}, \quad (17)$$

$$\sigma_{zx}^M: J_z(0,0) = \frac{i}{8\pi^2} \frac{\omega_{pi}^2}{\omega} \frac{\omega_{ci}}{c} \cdot \left(\frac{\omega}{|k_{\parallel} v_T} \right)^2 Z' \left(\frac{\omega}{|k_{\parallel} v_T} \right) \int_0^{2\pi} d\theta \int_0^{2v_0/\omega_{ci}} dr \cdot \frac{\omega_{ci}}{v_0} \frac{r}{\pi \sqrt{2^2 - \left(\frac{\omega_{ci} r}{v_0}\right)^2}} B_r(r, \theta). \quad (18)$$

In these equations current components J_x, J_y, J_z at the point $x=0, y=0$ are calculated in terms of integrals of field components $E_r, E_\theta, B_r, B_\theta$ calculated in polar coordinates r, θ such that $x=r \cos \theta, y=r \sin \theta$. The integration is limited to the area inside the circle with the radius equal to the Larmor diameter $L_0=2v_0/\omega_{ci}$ of ions.

The conductivity kernel components in Eqs. (15)–(18) are singular but integrable at $r=L_0$, following from $F(\mathbf{v}) \propto \delta(v_\perp - v_0)$. Also because of this kind of distribution function used in the calculations the response due to the σ_{yy}^E component involves not only E_r, E_θ but also $\partial E_\theta/\partial r$. For a regular distribution function the kernel is regular and one can avoid the presence of spatial derivatives inside the integral.

Because of a localized structure of eigenfunctions an enhanced numerical resolution is required in some cases for accurate integration.

Equations (15)–(18) can be simplified as follows. Using Maxwell equation

$$\nabla \times \mathbf{E}|_z = \frac{1}{r} \frac{\partial}{\partial r}(rE_\theta) - \frac{1}{r} \frac{\partial E_r}{\partial \theta} = \frac{i\omega}{c} B_z$$

one can express the combination of electric field components in Eq. (15) in terms of B_z . Then the change of variable

$$r=L_0 \sin \beta \tag{19}$$

reduces Eq. (15) to

$$\begin{bmatrix} J_x(0,0) \\ J_y(0,0) \end{bmatrix} = \frac{L_0}{4\pi^3} \frac{\omega_{pi}^2}{c} \cdot \frac{\omega}{|k_\parallel v_T} Z\left(\frac{\omega}{|k_\parallel v_T}\right) \int_0^{2\pi} d\theta \int_0^{\pi/2} d\beta \begin{pmatrix} \sin \theta \\ -\cos \theta \end{pmatrix} \sin \beta B_z(L_0 \sin \beta, \theta). \tag{20}$$

In a similar way the change of variable of Eq. (19) simplifies Eqs. (16)–(18). In these new variables the conductivity kernels are regular simple functions which are well suited for numerical integration.

In the above derivations we obtained analytical results for the conductivity kernels in x, y (or r, θ) coordinates. It seems that an analytical result cannot be obtained when one replaces one of the coordinates by its Fourier representation, for instance x, k_y combination.

Perpendicular electric field in the eigenmodes in Fig. 2 is mostly electrostatic. Particles current responding on the electrostatic part of the electric field is due to the σ_{yx}^E component. Equation (20) shows that the current due to σ_{yy}^E component is the response on electromagnetic part of perturbation. This

response can be comparable with the response on the dominant electrostatic part of the electric field because of the scaling $\sigma_{yx}^E \sim \epsilon \sigma_{yy}^E$ [see Eqs. (9) and (10)].

In order to use the fast particles response found in this section in the analysis of cylindrical eigenmodes with wave numbers m and k one should find the corresponding integral relations between the Fourier amplitudes in the global cylindrical coordinates (which are not connected with the point in which the perturbed current is considered). For this one should recalculate the above integral relations in global cylindrical coordinates and then make a Fourier transform of coordinate θ . One obtains the corresponding contributions to the current response

$$\sigma_{yy}^E : \begin{bmatrix} J_r^m(r) \\ J_\eta^m(r) \end{bmatrix} = \frac{\delta_1}{\pi^2} \tilde{L}_0 \int_0^{2\pi} d\tilde{\theta} \int_0^{\pi/2} d\beta \cdot \frac{\omega}{|k_\parallel v_T} Z\left(\frac{\omega}{|k_\parallel v_T}\right) \sin \beta \begin{pmatrix} \sin \tilde{\theta} \\ -\cos \tilde{\theta} \end{pmatrix} B_\parallel^m(r_1) e^{im\alpha},$$

$$\sigma_{xy}^E, \sigma_{yx}^E : \begin{bmatrix} J_r^m(r) \\ J_\eta^m(r) \end{bmatrix} = \frac{2\delta_1}{\pi^2} \frac{v_A}{a\omega_{ci}} \int_0^{2\pi} d\tilde{\theta} \int_0^{\pi/2} d\beta \sin^2 \beta \begin{pmatrix} \sin \alpha & \cos \alpha \\ -\cos \alpha & \sin \alpha \end{pmatrix} \begin{bmatrix} E_r^m(r_1) \\ E_\eta^m(r_1) \end{bmatrix} e^{im\alpha},$$

$$\begin{aligned} \sigma_{yx}^M : \begin{bmatrix} J_r^m(r) \\ J_\eta^m(r) \end{bmatrix} &= \frac{i\delta_1}{4\pi^2} \left(\frac{\omega_{ci}}{\omega}\right)^2 \tilde{L}_0^2 \int_0^{2\pi} d\tilde{\theta} \int_0^{\pi/2} d\beta k_\parallel \cdot \left(\frac{\omega}{|k_\parallel v_T}\right)^2 Z'\left(\frac{\omega}{|k_\parallel v_T}\right) e^{im\alpha} \\ &\times \begin{bmatrix} -\sin \tilde{\theta} \sin^2 \beta \cos(\alpha - \tilde{\theta}) + \cos \tilde{\theta} \cos^2 \beta \sin(\alpha - \tilde{\theta}) & \sin \tilde{\theta} \sin^2 \beta \sin(\alpha - \tilde{\theta}) + \cos \tilde{\theta} \cos^2 \beta \cos(\alpha - \tilde{\theta}) \\ \cos \tilde{\theta} \sin^2 \beta \cos(\alpha - \tilde{\theta}) + \sin \tilde{\theta} \cos^2 \beta \sin(\alpha - \tilde{\theta}) & -\cos \tilde{\theta} \sin^2 \beta \sin(\alpha - \tilde{\theta}) + \sin \tilde{\theta} \cos^2 \beta \cos(\alpha - \tilde{\theta}) \end{bmatrix} \\ &\times \begin{bmatrix} B_r^m(r_1) \\ B_\eta^m(r_1) \end{bmatrix}, \end{aligned}$$

$$\sigma_{zx}^M : J_\parallel^m(r) = \frac{i\delta_1}{2\pi^2} \frac{\omega_{ci}}{\omega} \tilde{L}_0 \int_0^{2\pi} d\tilde{\theta} \int_0^{\pi/2} d\beta \cdot \left(\frac{\omega}{|k_\parallel v_T}\right)^2 Z'\left(\frac{\omega}{|k_\parallel v_T}\right) \sin \beta [\cos(\alpha - \tilde{\theta}) B_r^m(r_1) - \sin(\alpha - \tilde{\theta}) B_\eta^m(r_1)] e^{im\alpha},$$

where $r_1 = \sqrt{(r + L_0 \sin \beta \cos \tilde{\theta})^2 + (L_0 \sin \beta \sin \tilde{\theta})^2}$, $\cos \alpha = (r + L_0 \sin \beta \cos \tilde{\theta})/r_1$, $\sin \alpha = L_0 \sin \beta \sin \tilde{\theta}/r_1$, $\tilde{L}_0 = L_0/a$, $\delta_1 = \omega_{p1}^2 a^2 / c^2$. In the above equations components of current, electric and magnetic fields are normalized as in the beginning of Sec. II. r_1 is the radial coordinate which is the function of variables of integration. The basis \mathbf{e}_r , \mathbf{e}_η , \mathbf{e}_\parallel is defined in Sec. II. In these equations recalculation in the global cylindrical coordinates is made with approximation that $\tilde{\mathbf{B}} \parallel \mathbf{z}$. The use of these equations for real RFP equilibrium is valid only when fast particles are not far from the magnetic axis. We assume that the density profile of fast particles is taken into account by a radial dependence of coefficient δ_1 .

In the above equations k_\parallel is now the function of r_1 defined in Sec. II. We moved the $k_\parallel(r)$ dependence inside the integrals due to the following. For an arbitrary spectrum of electric field the spectrum of current is $J(x_0, y_0, k_z) = \iint dx dy \sigma(x - x_0, y - y_0, k_z) E(x, y, k_z)$. The response of current on electric field of the form $E_1(x, y, z) = E_1(x, y) e^{ik(x, y)z}$ is $J(x_0, y_0, z) \propto \iint dx dy \sigma[x - x_0, y - y_0, k(x, y)] E_1(x, y) e^{ik(x, y)z}$. If $k(x, y)$ slowly varies with x, y one can assume $e^{ik(x, y)z} \approx e^{ik(x_0, y_0)z}$ which validates the insertion of $k_\parallel(r)$ dependence inside the integrals. For the $k_\parallel(r)$ profiles used in our analysis this approximation is justified for almost the whole range of the examined Larmor diameters L_0 . For a finite v_T in the distribution function of Eq. (8) the conductivity kernel strongly depends on k_\parallel in the vicinity of the resonance surface. The positioning of the dependence $k_\parallel(r)$ inside the integrals properly handles this situation.

IV. FAST PARTICLE CONTRIBUTION

We assume that the fast ion density is much smaller than the bulk density. We neglect the influence of fast ions on the plasma equilibrium, as well as the collisions between bulk particles and fast ions. The fast ions are considered as a separate plasma component which interacts with the plasma bulk only via the collective electromagnetic field.

If we assume that \mathbf{J} is the current of the plasma bulk then the contribution from fast particles changes only Eq. (5) in the set of Eqs. (2)–(5) such as

$$\nabla \times \mathbf{B} = \mathbf{J} + \mathbf{J}_f. \tag{21}$$

In this equation \mathbf{J}_f is the current response of fast particles on the specified perturbation of electromagnetic field. We neglect the contribution of the fast ions to Ohm's law. Hence the fast ions enter the MHD dynamics only through their influence on the perturbed magnetic field. The response, \mathbf{J}_f , is calculated in the preceding section. There is also a contribution from the electron component that compensates the charge of fast ions. Because of low density the response from this component is negligible relative to the response from bulk electrons. This component, however, makes a contribution when the $\mathbf{E} \times \tilde{\mathbf{B}}$ drift of the electrons in this component is not balanced by the drift of fast ions because of the FLR effects. This contribution is formally included in \mathbf{J}_f in Eq. (21) (we discuss it in Sec. V C). Equations (2)–(4), (21) formulate the eigenmode problem in the presence of fast particles.

We find the changes to the growth rates of unstable modes due to the presence of fast particles by two methods. First, assuming the fast particles response to be a correction to the MHD current we develop a perturbation technique for finding the changes to the growth rate. In a different approach based on a time evolution of an initial value problem we find an accurate solution with the presence of fast particles. In this approach the accurate solution is found for the σ_{yy}^E component of fast ions response. The exact time evolution method is numerically intensive and it is developed for one specific case (see the remark later in this section). We use the exact method to benchmark the perturbation technique, and then use the latter for the results.

In the perturbation technique the substitution of the form $B \rightarrow B + \tilde{B}, \dots, \omega \rightarrow \omega + \Delta\omega$ is made in Eqs. (2)–(4), (21), where B, ω relates to the eigenmode values without fast particles. As in Sec. II one can derive a set of equations for amplitudes $\tilde{B}_r, \tilde{B}_\eta, \tilde{B}_\parallel$ in the form in which the right-hand side in these equations contains terms proportional to $\Delta\omega$ (they contain combinations of the unperturbed field components) and terms containing components \mathbf{J}_f (these are calculated as a response on the unperturbed fields of the eigenmode).

The general solution of these equations is

$$\begin{pmatrix} \tilde{B}_\eta \\ \tilde{B}_\parallel \end{pmatrix} = C_1 \begin{pmatrix} B_\eta^1 \\ B_\parallel^1 \end{pmatrix} + C_2 \begin{pmatrix} B_\eta^2 \\ B_\parallel^2 \end{pmatrix} + \begin{pmatrix} B_\eta^f \\ B_\parallel^f \end{pmatrix} + \Delta\omega \begin{pmatrix} B_\eta^\Delta \\ B_\parallel^\Delta \end{pmatrix}. \tag{22}$$

The coefficients C_1 and C_2 in this solution are arbitrary. Functions B_η^1, B_\parallel^1 and B_η^2, B_\parallel^2 are the solutions of uniform equations corresponding to boundary conditions on the resonance surface $B_\eta^1(r_s) = 1, B_\parallel^1(r_s) = 0$ and $B_\eta^2(r_s) = 0, B_\parallel^2(r_s) = 1$. Functions B_η^f, B_\parallel^f and $B_\eta^\Delta, B_\parallel^\Delta$ are the particular solutions of nonuniform set of equations corresponding to the right-hand-side terms which contain components \mathbf{J}_f and which are proportional to $\Delta\omega$, respectively. These solutions are calculated with the boundary conditions $B_\eta^f(r_s) = B_\parallel^f(r_s) = 0, B_\eta^\Delta(r_s) = B_\parallel^\Delta(r_s) = 0$.

With the help of the solution of Eq. (22) one can find the total plasma current in two regions $0 \leq r < r_s$ and $r_s < r \leq 1$. Matching the tangential components of the total current at $r = r_s$ leads to an algebraic nonuniform set of equations for the coefficients C_1 and C_2 . Because the functions with superscripts “1” and “2” are the solutions of unperturbed problem, the determinant of the set of equations for C_1 and C_2 is zero. In order for this system of equations to have a solution, it is necessary that the rank of the coefficient matrix be equal to the rank of its augmented matrix. This condition leads to the equation for $\Delta\omega$.

In a different approach we solve time dependent resistive MHD equations combined with Eq. (21) as an initial value problem. We solve this problem in this way only for the fast ions response due to σ_{yy}^E component of the conductivity tensor and only in the limit $v_T = 0$. In this case the current response of Eq. (20) is local in time (it does not depend on frequency ω) which simplifies the solution method. The initial value problem is solved numerically by an explicit predictor–corrector method.

TABLE I. Comparison of results of perturbation method with exact solution.

Without fast particles		Changes to the growth rate due to fast particles	
Equilibrium	$\gamma\tau_A$	$\Delta\gamma\tau_A$ perturbation method	$\Delta\gamma\tau_A$ exact
$\alpha_0=2, \Theta_0=2$ $ka=-2.3$	1.73×10^{-2}	-0.162×10^{-2}	-0.14×10^{-2}
$\alpha_0=2.6, \Theta_0=1.8$ $ka=-2$	9.56×10^{-3}	-2.89×10^{-3}	-2.1×10^{-3}
$\alpha_0=3, \Theta_0=1.75$ $ka=-2$	1.1×10^{-3}	-1.34×10^{-3}	Stable

We compare the results of perturbation method with the exact results from the time evolution approach. We consider changes to the growth rate due to σ_{yy}^E component of fast particles response. Table I shows the growth rates for three unstable equilibria C, B, A in Fig. 1 without fast particles and the changes to the growth rates due to fast particles calculated by the perturbation method and by the exact time evolution method. For each case $m=1, v_T=0, L_0/a=0.3, S=10^4$, fast particles density profile

$$n_f = \begin{cases} 2 \times \left[1 - \left(\frac{r/a}{0.35} \right)^3 \right] \times 10^{11} \text{ cm}^{-3}, & r/a \leq 0.35, \\ 0, & r/a > 0.35. \end{cases}$$

The wave numbers k are chosen such that for each equilibrium in Table I the location of resonance surface is approximately at $r_s=0.3$. The density profile of fast particles covers the resonance surface. In accordance with the restrictions of the model fast particles are distributed not far from magnetic axis.

For the cases when $\Delta\gamma$ is small relative to the unperturbed growth rate γ the perturbation method result is close to the exact result. When $\Delta\gamma$ is comparable to γ the results of the two methods show similar trends. For the least unstable equilibrium in Table I, the perturbation method gives the stabilizing correction to the growth rate which is larger than the growth rate itself, while the exact solution corresponds to the stabilized mode. Thus the perturbation method is appropriate for qualitative analysis. With this method one can estimate the strength and the direction of the effect. In the next section the effects of fast particles will be examined using the perturbation method.

V. RESULTS

In this section we analyze the changes to the growth rates of the unstable modes due to fast particles. We apply the perturbation method discussed in the preceding section. We consider the effects from each component of the conductivity tensor of Eqs. (9)–(12) separately. Some components of the conductivity tensor are specific to the highly anisotropic distribution function of Eq. (8) used in our analysis (they disappear in the isotropic case) while others preserve their property when a transition to isotropic distribution function is made. In a separate analysis of each component one can make some assumptions about the results when a

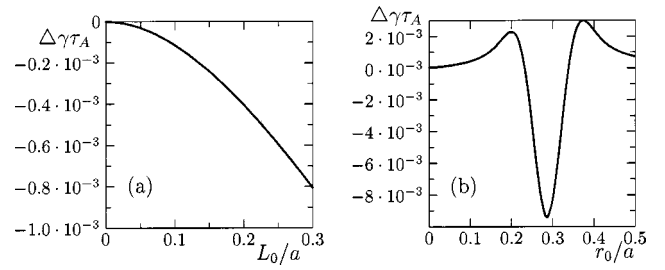


FIG. 3. Changes to the growth rate ($\Delta\gamma$) due to σ_{yy}^E component. (a) $\Delta\gamma$ vs normalized gyrodiameter L_0/a for $n_f=2 \exp[-(r/(0.45a))^2] \times 10^{11} \text{ cm}^{-3}$; (b) $\Delta\gamma$ vs peak radius of fast ion density distribution r_0/a for $n_f=2 \times \exp[-[(r-r_0)/0.05a]^2] \times 10^{11} \text{ cm}^{-3}$, $L_0/a=0.3$. In both cases $\alpha_0=3, \Theta_0=1.75, m=1, ka=-2, v_T/v_0=0, S=10^4, \gamma\tau_A=1.10 \times 10^{-3}$. The mode resonant surface is located at $r/a \approx 0.3$.

more general distribution function is used. In this section we consider plasma bulk equilibrium described in Sec. II with uniform density profile $n(r)=10^{13} \text{ cm}^{-3}$.

A. σ_{yy}^E component

We consider a case appropriate for the MST experiment with magnetic field $B=3 \text{ kG}$. Fast hydrogen ions with energy 20 keV have Larmor diameter $L_0/a \approx 0.3$ for $a=50 \text{ cm}$. The fast ion response due to the σ_{yy}^E component contains the component B_{\parallel} in the integral over the area limited by the Larmor diameter (see Sec. III). For the profiles of B_{\parallel} corresponding to the cylindrical eigenmodes shown in Fig. 2 fast ion current, calculated for a typical Larmor diameter of neutral beam injected particles, is a smooth function of radius everywhere including the vicinity of resonance surface. The field component B_{\parallel} does not change sign at the resonance so that there is no cancellation of terms during the integration. The current is as strong near the resonance as in the outer region.

In the following cases we select equilibrium A ($\alpha_0=3, \Theta_0=1.75$) of Fig. 1 and evaluate the changes to the eigenmode with wave numbers $m=1$ and $ka=-2$. Figure 3(a) shows the changes to the growth rate $\Delta\gamma$ versus normalized Larmor diameter L_0/a . The correction to the eigenfrequency is purely imaginary, only the growth rate is changed. We have chosen the fast particle density profile as

$$n_f = 2 \exp \left[- \left(\frac{r}{0.45a} \right)^2 \right] \times 10^{11} \text{ cm}^{-3} \quad (23)$$

with $v_T/v_0=0, S=10^4$ and the unperturbed growth rate $\gamma\tau_A=1.10 \times 10^{-3}$. The fast particle density profile n_f covers the resonance surface which is located near $r/a=0.3$. The dependence of $\Delta\gamma$ on L_0 in Fig. 3(a) is approximately quadratic. The effect is sizable; $\Delta\gamma$ is comparable with γ for the realistic Larmor diameter and the density of fast particles. For this radial profile of fast particles density the effect is stabilizing. The contribution from fast ions is due to FLR effects, disappearing in the limit $L_0 \rightarrow 0$.

We examine the influence of the radial location of the fast particles by considering a narrow distribution $n_f = 2 \exp[-[(r-r_0)/0.05a]^2] \times 10^{11} \text{ cm}^{-3}$, and varying r_0 . For the linear problem $\Delta\gamma$ corresponding to a realistic density profile is a superposition of parts due to different narrow

density profiles. $\Delta\gamma$ calculated for the particular narrow density profile centered at $r=r_0$ approximately shows the contribution from the fast particles located at this point. Figure 3(b) shows the dependence of $\Delta\gamma$ on r_0/a for $L_0/a=0.3$. The other parameters are the same as in Fig. 3(a). There is a strong influence on $\Delta\gamma$ from fast particles distributed near the resonance surface. Thus for the contribution from σ_{yy}^E component the result strongly depends on the presence of fast particles at the resonance surface. The slowly varying near resonance surface perpendicular fast particles current due to this component of the conductivity tensor tends to stabilize the mode. In general, the effect is stabilizing for the distributions which cover the resonance surface. Results similar to those presented in Figs. 3(a) and 3(b) but with different scales are obtained for other equilibria and different Lundquist numbers. The relative changes to the growth rate for more unstable equilibria are weaker.

In the cases when the Larmor diameter is specified in our calculations its value corresponds to the realistic energy of NBI particles in the RFP. In these conditions the assumption of uniformity of equilibrium field within the gyro-orbit is not accurate. Results of calculations with smaller Larmor diameters are similar to those presented in the paper with the only difference being that the changes to the growth rate are smaller. Extension of the model to the larger Larmor diameters provides a qualitative trend of the strength of the effect which is in line with the use of the perturbation method for the qualitative analysis.

The fast particle distribution is flat when compared with the strongly localized components of plasma velocity and electric field in the eigenmode. As a result of the introduction of the fast particle component an additional volume force $\delta\mathbf{f}(r)$ is exerted on the plasma bulk. The force $\delta\mathbf{f}(r)$ relates to the correction to the right-hand side in Eq. (3) due to the perturbation of magnetic field and bulk current when the fast particles are added. The radial spread of this force is wider than the resonant region and its shape roughly repeats the radial distribution of fast particles. The work done by the force $\delta\mathbf{f}(r)$ on the plasma per unit time is $\int \delta\mathbf{f}(r) \cdot \mathbf{v}(r) dr$, where $\mathbf{v}(r)$ is the velocity profile in the unperturbed eigenmode. Because $\mathbf{v}(r)$ is localized near the resonance the contribution to the integral is strongest from $\delta\mathbf{f}(r)$ near the resonance. Thus one should expect that the strongest effect on the eigenmode is from particles distributed near the resonance. The width of profiles $\Delta\gamma$ versus r_0 is determined by the width of test function $n_f(r)$ used in Fig. 3(b) which is wider than the unperturbed eigenfunctions near the resonance.

We examine the effect for different Lundquist numbers. Figure 4(a) shows the dependence of $\Delta\gamma/\gamma$ on S for the density profile of Eq. (23). The ratio $|\Delta\gamma|/\gamma$ reduces with the increase of S . This is probably due to the narrowing of the resistive (reconnection) layer width which reduces the influence of fast particles within this region. For the more unstable equilibria *B* and *C* in Fig. 1 the ratios $|\Delta\gamma|/\gamma$ for $S=10^4$ are smaller than for the same conditions in equilibrium *A*. For equilibria *B* and *C*, however, $\Delta\gamma/\gamma$ changes slightly with the increase of S up to the largest examined value $S=5 \times 10^5$.

For finite v_T the effect of parallel temperature is in-

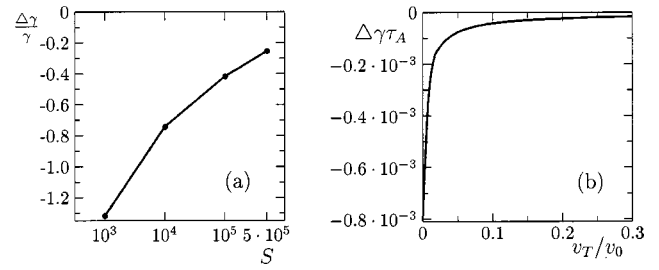


FIG. 4. Changes to the growth rate due to σ_{yy}^E component. (a) $\Delta\gamma/\gamma$ vs Lundquist number S for $v_T/v_0=0$; (b) $\Delta\gamma/\gamma$ vs v_T/v_0 for $S=10^4$. In both cases $\alpha_0=3$, $\Theta_0=1.75$, $m=1$, $ka=-2$, $n_f=2 \exp[-(r/0.45a)^2] \times 10^{11} \text{ cm}^{-3}$, $L_0/a=0.3$.

cluded in the coefficient $-(\omega/k_{\parallel}|v_T)Z(\omega/k_{\parallel}|v_T)$ in the equation for fast particles current. Because of the relatively small growth rate $\gamma \propto |\omega|$ this coefficient is a small factor for finite realistic v_T everywhere except near the resonance surface where $k_{\parallel}(r) \rightarrow 0$. The suppression of the response is due to the phase mixing in velocity integral occurring when particle's velocity is larger than the phase velocity of the perturbation. Figure 4(b) shows the dependence of $\Delta\gamma$ on v_T/v_0 for the density profile of Eq. (23). $|\Delta\gamma|$ decreases rapidly with the increase of v_T/v_0 . The effect diminishes with finite parallel temperature. Within the considered model the contribution from σ_{yy}^E component is suppressed for a realistic spread of parallel velocity of neutral beam particles injected perpendicularly to magnetic field. In a more realistic model including particle trapping the effect from this component could survive. Also the effect should be stronger in tokamaks because of the smaller value of k_{\parallel} (from the weaker magnetic shear) of the core resonant modes.

B. σ_{yx}^M component

The fast ion current response due to the σ_{yx}^M component appears because of anisotropy of the distribution function. In the limit $v_T \rightarrow 0$ this response is proportional to ω^{-2} [see Eq. (17)]. Because of the relative smallness of the growth rates this response is very strong. The current response on the given perturbation of magnetic field is a smooth function of radius everywhere in the plasma. There is no suppression of the response at the resonance surface since B_{η} is not oscillatory with radius. Because the response is strong we consider the changes to the growth rate for the most unstable equilibrium *C* in Fig. 1.

For this component we perform similar analysis as for the component σ_{yy}^E . In the following cases we consider the equilibrium *C* ($\alpha_0=2$, $\Theta_0=2$) with $m=1$, $ka=-2.3$. Figure 5(a) shows the dependence of $\Delta\gamma$ on L_0/a for fast particles density profile of Eq. (23). The unperturbed growth rate is $\gamma\tau_A=1.73 \times 10^{-2}$. The correction to the eigenfrequency is purely imaginary. In Fig. 5(a) $\Delta\gamma$ is approximately proportional to L_0^4 . The effect is very strong; $\Delta\gamma$ is much larger than γ for realistic Larmor diameter and fast particles density. Because of the strong effect the perturbation method is invalid. However one should expect a strong stabilizing effect for this fast particle density profile. Figure 5(b) shows

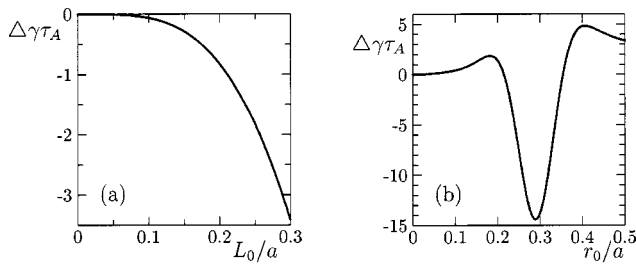


FIG. 5. Changes to the growth rate ($\Delta\gamma$) due to σ_{yx}^M component. (a) $\Delta\gamma$ vs normalized gyrodiameter L_0/a for $n_f = 2 \exp[-(r/0.45a)^2] \times 10^{11} \text{ cm}^{-3}$; (b) $\Delta\gamma$ vs peak radius of fast ion density distribution r_0/a for $n_f = 2 \times \exp[-[(r-r_0)/0.05a]^2] \times 10^{11} \text{ cm}^{-3}$, $L_0/a = 0.3$. In both cases $\alpha_0 = 2$, $\Theta_0 = 2$, $m = 1$, $ka = -2.3$, $v_T/v_0 = 0$, $S = 10^4$, $\gamma\tau_A = 1.73 \times 10^{-2}$. The mode resonant surface is located at $r/a \approx 0.3$.

that the effect is strongly influenced by the presence of fast particles near the resonance surface. The effects due to this component dominate the other contributions.

Figure 6(a) shows the dependence of $\Delta\gamma/\gamma$ on S for the density profile of Eq. (23). The absolute value of $\Delta\gamma/\gamma$ strongly increases with S . This increase is due to the strong frequency (growth rate) dependence of current response in Eq. (17). The effect of parallel temperature is included in the coefficient $(\omega/|k_{\parallel}v_T)^2 Z'(\omega/|k_{\parallel}v_T)$ in the equation for the fast particle current. For finite realistic v_T this coefficient is a small factor everywhere except near the resonance surface. Figure 6(b) shows that $|\Delta\gamma|$ decreases with v_T/v_0 . For the considered parameters $\Delta\gamma$ changes sign at some value of v_T/v_0 . For the realistic values of v_T , $\Delta\gamma$ is much smaller than the one calculated in the limit $v_T = 0$ but its value is comparable with the unperturbed growth rate. Thus finite parallel temperature reduces the effect, but it remains strong. This reduction of the effect can be smaller in a more realistic model which includes the effects of trapped particles.

C. σ_{xy}^E , σ_{yx}^E , and σ_{zx}^M components

The fast ion response due to σ_{xy}^E and σ_{yx}^E components is calculated at the end of Sec. III. The response contains the integral of electric field components E_r , E_{η} which are localized near the resonance surface (see Fig. 2). The dominant component, E_r , oscillates near the point $r = r_s$. This leads to the cancellation of terms inside the integral. Thus for relatively large Larmor diameters the fast particle response due

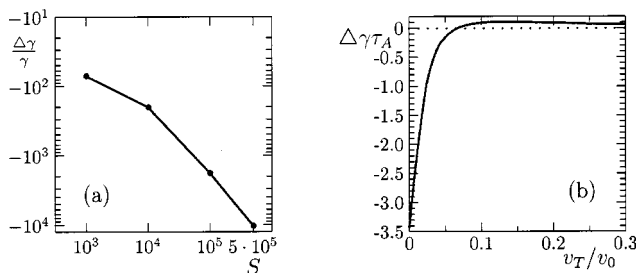


FIG. 6. Changes to the growth rate due to σ_{yx}^M component. (a) $\Delta\gamma/\gamma$ vs Lundquist number S for $v_T/v_0 = 0$; (b) $\Delta\gamma$ vs v_T/v_0 for $S = 10^4$. In both cases $\alpha_0 = 2$, $\Theta_0 = 2$, $m = 1$, $ka = -2.3$, $n_f = 2 \exp[-(r/0.45a)^2] \times 10^{11} \text{ cm}^{-3}$, $L_0/a = 0.3$.

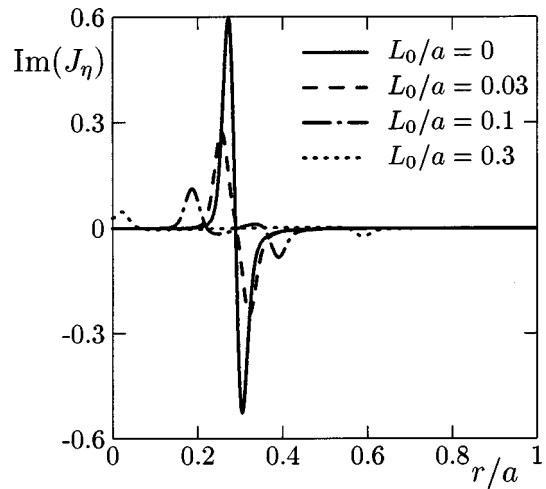


FIG. 7. Fast ion current component J_{η} (in arbitrary units) vs r/a for different normalized Larmor diameters L_0/a due to σ_{xy}^E , σ_{yx}^E components.

to these components of the conductivity tensor is suppressed. Figure 7 demonstrates this result. It shows the dominant component of fast ion current J_{η} for different Larmor diameters L_0/a for a flat fast particles density profile and $v_T/v_0 = 0$. The current is a response to electric field components presented in Fig. 2(b). Figure 7 shows that the response is largest when $L_0 \rightarrow 0$. In this limit the response is local with respect to the radial coordinate, and the current component repeats the shape of the profile of electric field component E_r in Fig. 2(b). In this limit the conductivity tensor reduces to the collisionless cold plasma conductivity tensor. With the increase of L_0/a the response diminishes such that for realistic Larmor diameters of fast particles in RFP one can neglect fast particles current relative to the current calculated in the limit $L_0 \rightarrow 0$. In a two fluid description at low frequency the ion $\mathbf{E} \times \bar{\mathbf{B}}$ drift is compensated by the electron $\mathbf{E} \times \bar{\mathbf{B}}$ drift such that the conductivity tensor components σ_{xy}^E , σ_{yx}^E corresponding to ions and electrons cancel each other. In our case the fast ion response is suppressed for realistic L_0 due to FLR effects. The combined response from the electron component that compensates the charge of fast ions and the fast ions is the uncompensated $\mathbf{E} \times \bar{\mathbf{B}}$ drift of electrons. This combined result does not change during the transition to isotropic distribution function.

We applied the perturbation method to examine the effect of the above combined response on the plasma eigenmode. Our calculations show that the correction $\Delta\omega$ to the eigenmode frequency is purely real so that there is no changes to the growth rate. Also the absolute value of $\Delta\omega$ is small relative to the changes to the growth rate calculated for the component σ_{yy}^E (for $v_T = 0$) under similar conditions. Thus the response due to σ_{xy}^E and σ_{yx}^E components changes somewhat the dispersion relation of the eigenmode but does not have stabilizing or destabilizing influence within the considered model.

Comparison of components σ_{zx}^M and σ_{yx}^M of Eqs. (12) and (11) shows that σ_{yx}^M component is dominant among the two unless k_{\parallel} is sufficiently small. We kept the σ_{zx}^M component in our analysis because it can be comparable with the σ_{yx}^M com-

ponent in the vicinity of resonance surface. Insertion of k_{\parallel} inside the integral discussed in Sec. III makes the response due to σ_{yx}^M component dominant in the resonance surface region as well for realistic Larmor diameters. Result of perturbation method analysis shows that $\Delta\omega$ due to the σ_{zx}^M component is purely real and is much smaller than $|\Delta\gamma|$ due to the σ_{yx}^M component for the same conditions. Therefore one can neglect the effects due to σ_{zx}^M component in comparison with the effects due to σ_{yx}^M component of the conductivity tensor.

VI. SUMMARY AND DISCUSSION

We studied the FLR effects in the modeling of fast particles component on internal modes in RFPs. We concentrated on a highly anisotropic fast particle distribution function with large perpendicular energy. We treat the effect of nonuniformity of the eigenfunction fields within a gyro-orbit (although, for simplicity we consider the equilibrium magnetic field to be uniform within a gyro-orbit). Our results show that pure FLR effects are sizable such that unstable modes with realistic growth rates can be strongly affected by the NBI injected fast particles with realistic parameters. We found that the effect is strongest for the fast particle response described by the σ_{yx}^M component of the conductivity tensor. The response due to this component is specific to the anisotropic distribution function. Also a sizable effect is found for the response due to the σ_{yy}^E component of conductivity tensor. This component is responsible for transit time magnetic pumping, which is the FLR effect that survives in waves in the limit of low frequency. The effects due to this component potentially survive the transition to an isotropic distribution function. The effect on stability arises from the perturbed Lorentz force contributed by the fluctuating fast particle current. The specific physical origin of the current, a response to the perturbed electric and magnetic fields, is complex since the response of the large-orbit particles is nonlocal. Finite parallel velocity in the distribution function reduces the effects from both components within our model, due to phase mixing in the velocity integral that occurs when the particle velocity is larger than the phase velocity of the perturbation. In a more realistic model accounting for particles trapping this reduction is probably less significant. The main result of our study is the demonstration of the significance of the FLR effects in the fast particle response in RFPs. More accurate modeling is required, however, to make quantitative predictions.

The Larmor radii of fast ions in the MeV energy range corresponding to ICRH heated ions or alpha particles in

burning plasmas in tokamaks are comparable with the typical radii examined here. Based on this comparison we suggest that the FLR effects can be important in these two cases.

ACKNOWLEDGMENTS

This work was supported by the U.S. Department of Energy and by the National Science Foundation Center for Magnetic Self-Organization in Laboratory and Astrophysical Plasmas.

APPENDIX: CONTRIBUTION TO THE CONDUCTIVITY KERNEL FROM $\sigma_{yy}^E(\mathbf{k}, \omega)$ COMPONENT

The components of the conductivity tensor of Eqs. (9)–(12) are found in the coordinates in which $\mathbf{k}_{\perp} \parallel \mathbf{e}_x$. Applying the tensor transformation rules one can find the conductivity tensor corresponding to the component $\sigma_{yy}^E(\mathbf{k}, \omega)$ of Eq. (9) for a general orientation of \mathbf{k}_{\perp} , $\mathbf{k}_{\perp} = k_{\perp}(\cos \varphi, \sin \varphi, 0)$,

$$\begin{aligned} \sigma_{ij}(\mathbf{k}, \omega) &= \sigma_{yy}^E(k_{\perp}, \omega) \cdot \begin{pmatrix} \sin^2 \varphi & -\sin \varphi \cos \varphi \\ -\sin \varphi \cos \varphi & \cos^2 \varphi \end{pmatrix} \\ &= \sigma_{yy}^E(k_{\perp}, \omega) \cdot \Phi_{ij}, \end{aligned}$$

where $i = x, y$, $j = x, y$.

The conductivity kernel can be obtained from its Fourier transform

$$\sigma_{ij}(x, y) = \frac{1}{(2\pi)^2} \int_{-\infty}^{\infty} \int_{-\infty}^{\infty} dk_x dk_y \sigma_{ij}(k_x, k_y) e^{-ik_x x - ik_y y}.$$

Changing the variables

$$k_x = k_{\perp} \cos \varphi, \quad k_y = k_{\perp} \sin \varphi$$

we find

$$\begin{aligned} \sigma_{ij}(x, y) &= \frac{1}{(2\pi)^2} \int_0^{\infty} dk_{\perp} k_{\perp} \int_0^{2\pi} d\varphi \sigma_{yy}^E(k_{\perp}, \omega) \Phi_{ij}(\varphi) \\ &\quad \times e^{-ik_{\perp}(x \cos \varphi + y \sin \varphi)}. \end{aligned}$$

We introduce cylindrical coordinates

$$x = r \cos \theta, \quad y = r \sin \theta$$

and use

$$e^{-ik_{\perp} r \cos(\varphi - \theta)} = \sum_n J_n(k_{\perp} r) \cdot e^{-in\pi/2 + in\theta - in\varphi}.$$

Then after integration over φ we obtain

$$\sigma_{ij}(r, \theta) = \frac{1}{4\pi} \int_0^{\infty} dk_{\perp} k_{\perp} \sigma_{yy}^E(k_{\perp}, \omega) \begin{pmatrix} J_0(k_{\perp} r) + J_2(k_{\perp} r) \cos 2\theta & J_2(k_{\perp} r) \sin 2\theta \\ J_2(k_{\perp} r) \sin 2\theta & J_0(k_{\perp} r) - J_2(k_{\perp} r) \cos 2\theta \end{pmatrix}.$$

Transforming to cylindrical basis

$$E_x = E_r \cos \theta - E_{\theta} \sin \theta,$$

$$E_y = E_r \sin \theta + E_{\theta} \cos \theta,$$

and using the recurrence formulas for the Bessel functions¹⁰ we get

$$\sigma_{ij}(r, \theta) = \frac{1}{2\pi} \int_0^\infty dk_\perp k_\perp \sigma_{yy}^E(k_\perp, \omega) \begin{pmatrix} \frac{J_1(k_\perp r)}{k_\perp r} \cos \theta & -J_1'(k_\perp r) \sin \theta \\ \frac{J_1(k_\perp r)}{k_\perp r} \sin \theta & J_1'(k_\perp r) \cos \theta \end{pmatrix},$$

where $i = x, y, j = r, \theta$. Now

$$J_i(0,0) = \int_0^{2\pi} d\theta \int_0^\infty dr r \sigma_{ij}(r, \theta) E_j(r, \theta)$$

with

$$\begin{aligned} \int_0^\infty dr r \sigma_{ij}(r, \theta) E_j(r, \theta) &= \frac{-i}{(2\pi)^2} \frac{\omega_{pi}^2}{\omega} \cdot \frac{\omega}{|k_\parallel v_T} Z\left(\frac{\omega}{|k_\parallel v_T}\right) \left\{ \int_0^\infty dr \int_0^\infty dk_\perp \xi_{\perp 0} J_0(\xi_{\perp 0}) J_1(\xi_{\perp 0}) J_1(k_\perp r) \begin{pmatrix} \cos \theta \\ \sin \theta \end{pmatrix} E_r \right. \\ &\quad \left. + \int_0^\infty dr r \int_0^\infty dk_\perp k_\perp \xi_{\perp 0} J_0(\xi_{\perp 0}) J_1(\xi_{\perp 0}) J_1'(k_\perp r) \begin{pmatrix} -\sin \theta \\ \cos \theta \end{pmatrix} E_\theta \right\}. \end{aligned}$$

The integral over k_\perp can be taken in the first term by using Eq. (13). The integral over k_\perp in the second term diverges. This divergence is because we use nonregular distribution function proportional to $\delta(v_\perp - v_0)$. The divergence can be removed by interchanging the order of integration (which corresponds to the initial integral relations). We rewrite the second term as

$$\begin{aligned} \int_0^\infty dr r \int_0^\infty dk_\perp k_\perp \xi_{\perp 0} J_0(\xi_{\perp 0}) J_1(\xi_{\perp 0}) J_1'(k_\perp r) E_\theta &= \int_0^\infty dk_\perp k_\perp \xi_{\perp 0} J_0(\xi_{\perp 0}) J_1(\xi_{\perp 0}) \int_0^\infty dr r J_1'(k_\perp r) E_\theta \\ &= - \int_0^\infty dk_\perp \xi_{\perp 0} J_0(\xi_{\perp 0}) J_1(\xi_{\perp 0}) \int_0^\infty dr J_1(k_\perp r) \frac{\partial [r E_\theta(r, \theta)]}{\partial r} \\ &= - \int_0^\infty dr \int_0^\infty dk_\perp \xi_{\perp 0} J_0(\xi_{\perp 0}) J_1(\xi_{\perp 0}) J_1(k_\perp r) \frac{\partial [r E_\theta(r, \theta)]}{\partial r} \\ &= - \int_0^{2v_0/\omega_{ci}} dr \cdot \frac{\omega_{ci}}{v_0} \frac{1}{\pi \sqrt{2^2 - \left(\frac{\omega_{ci} r}{v_0}\right)^2}} \frac{\partial [r E_\theta(r, \theta)]}{\partial r}. \end{aligned}$$

The combined result from the two terms is Eq. (15).

¹F. Porcelli, Plasma Phys. Controlled Fusion **33**, 1601 (1991).

²B. Coppi, S. Migliuolo, and F. Porcelli, Phys. Fluids **31**, 1630 (1988).

³B. Coppi and S. Migliuolo, Phys. Fluids B **2**, 927 (1990).

⁴A. Ödöblom, B. N. Breizman, S. E. Sharapov, T. C. Hender, and V. P. Pastukhov, Phys. Plasmas **9**, 155 (2002).

⁵R. N. Dexter, D. W. Kerst, T. W. Lovell, S. C. Prager, and J. C. Sprott, Fusion Technol. **19**, 131 (1991).

⁶M. Brambilla, Plasma Phys. Controlled Fusion **43**, 483 (2001).

⁷S. Ortolani and D. Schnack, *Magnetohydrodynamics of Plasma Relaxation* (World Scientific, Singapore, 1993).

⁸V. Antoni, D. Merlin, S. Ortolani, and R. Paccagnella, Nucl. Fusion **26**, 1711 (1986).

⁹M. Brambilla, *Kinetic Theory of Plasma Waves, Homogeneous Plasmas* (Oxford University Press, Oxford, 1998).

¹⁰E. T. Whittaker and G. N. Watson, *Modern Analysis* (Cambridge University Press, London, 1952).